[8]H. Höchst, S. Hüfner, and A. Goldman, Phys. Lett. 57A, 265 (1976).
[9]These binding energies are in exact agreement with those reported in G. Apai *et al.*, Solid State Comun. 20, 1141 (1976). However, in P. R. Norton and P. J. Richards, Surf. Sci. 49, 567 (1975), 9.1 eV is given as the binding energy for 5σ-1π levels ($h\nu$=40 eV) which may be due to cross-sectional variations as a function of photon energy and/or angular electron-emission effects.
[10]U. Gelius, E. Basilier, S. Svensson, T. Bergmark, and K. Siegbahn, J. Electron. Spectrosc. 2, 40(S) (1973).
[11]P. R. Norton, R. L. Tapping, and J. W. Goodale, Chem. Phys. Lett. 41, 247 (1976).
[12]G. W. Rubloff, W. D. Grobman, and H. Lüth, Phys. Rev. B 14, 1450 (1976).
[13]P. R. Norton and R. L. Tapping, Chem. Lett. 38, 207 (1976).
[14]J. W. Gadzuk, Phys. Rev. B 14, 2267 (1976).
[15]P. S. Bagus and K. Hermann, Solid State Commun. 20, 5 (1976).
[16]D. S. Rajoria, L. Kovnat, E. W. Plummer, and W. R. Salaneck, to be published; E. W. Plummer, W. R. Salaneck, and J. S. Miller, to be published.
[17]S. Doniach and M. Sunjic, J. Phys. C 3, 285 (1970); S. Doniach, private communication.
[18]P. S. Bagus and E. K. Viinikka, Phys. Rev. A 15, 1486 (1977).

Dispersion of Electronic Surface Resonances and Crystal Surface Structure

E. G. McRae, J. M. Landwehr, and C. W. Caldwell
Bell Laboratories, Murray Hill, New Jersey 07974
(Received 6 January 1977; revised manuscript received 21 March 1977)

A new method of determining the lateral structure of crystal surfaces is described. The dispersion of electronic surface resonances at energies of the order of 10 eV above the vacuum level is measured, and the results are interpreted using a nearly free-electron method to determine low-index Fourier coefficients of the potential acting on electrons near the surface. The method is shown to reproduce the known lateral structure of Ni(001)$c(2\times2)$O surface.

The determination of atomic arrangements at crystal surfaces is one of the outstanding problems of surface physics. The methods that have been applied successfully to this problem, low-energy-electron-diffraction (LEED) intensity analysis[1] and angle-resolved ultraviolet photoelectron spectroscopy (UPS),[2] have drawbacks of cost and of complexity of interpretation that place them beyond the resources of all but a few institutions. There is a need for a method of surface-structure determination that is experimentally simple and that does not present very difficult or costly problems of interpretation. Such a method is described in this Letter.

The method consists of measuring the dispersion of electronic surface resonances (the surface-resonance band structure) at energies of the order of 10 eV above the vacuum level. By application to a surface whose structure is already known from LEED, namely Ni(001)$c(2\times2)$O,[3] we demonstrate that (a) resonance dispersion curves can be interpreted in a simple way to determine the lateral variation of potential acting on electrons at the surface, and (b) the potential is related in a straightforward way to the lateral geometrical arrangement of surface atoms.

The physical mechanism underlying the method is one of resonant elastic scattering of electrons incident on the crystal from vacuum.[4-6] The incident electrons are trapped in a temporary surface state and subsequently released without change of energy. This kind of resonant scattering is known from a variety of low-energy-electron scattering experiments.[7-9] In the present experiment, resonances are observed as narrow fluctuations of the electron reflection coefficient with respect to variation of incident electron energy and incident direction. The dispersion is determined by entering the locations of the fluctuations on a plot of energy E against reduced parallel momentum $\vec{k}_{\parallel}$ of the incident electrons.

The experimental method consists of measuring the net current passing between the cathode of an electron gun and a crystal mounted in front of it in a conventional LEED apparatus.[8,10] A retarding field is used to help focus the beam as described previously.[7,10] The electron energy is obtained from the accelerating potential by subtracting an experimentally determined contact potential difference. The experiment is arranged so that variations of the negative of the net current are proportional to variations of the reflection coefficient.

In order to locate the resonance fluctuations

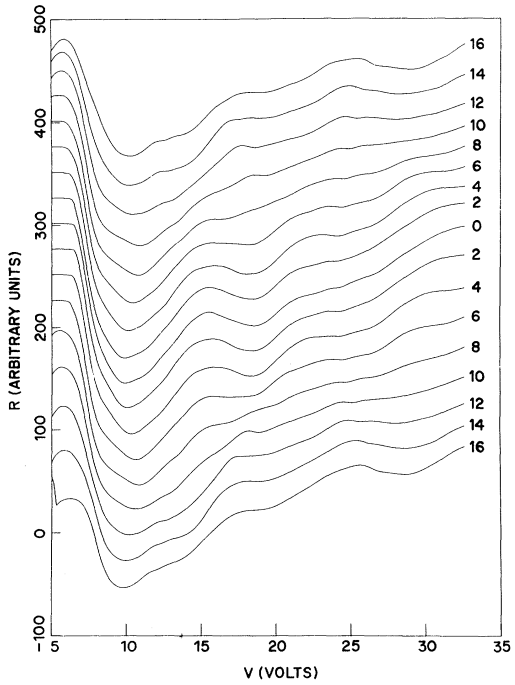

FIG. 1. Plots of R, the negative of the net current, vs accelerating potential V for Ni(001)$c(2\times2)$O surface. Plots are shown for each of a sequence of angular settings of the crystal with respect to rotation about its [110] axis. Results for both senses of rotation are presented as a check of the normal-incidence setting. Nominal angles of incidence from the angular settings (degrees) are shown by numbers against each curve.

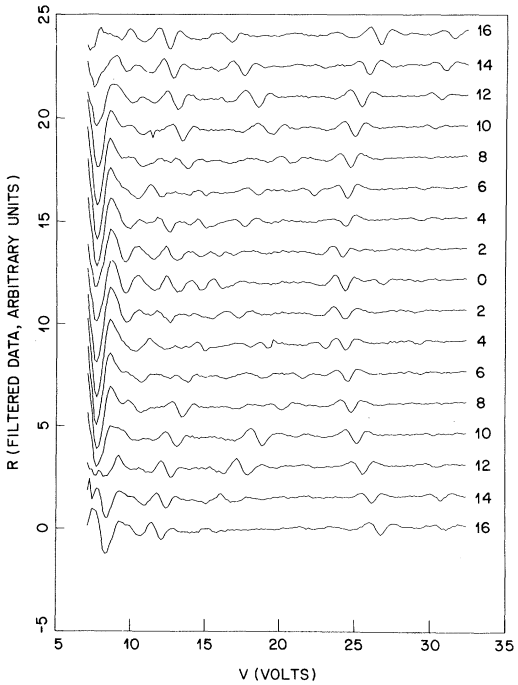

FIG. 2. The data of Fig. 1 after filtering to remove background.

with the needed precision, we obtain net-current data in digital form[11] and use a high-pass digital filter to remove the background due to inelastic and nonresonant elastic scattering. The filtered series is obtained by convolving the data series with the filter coefficients. A filter approximating a perfect high-pass filter was constructed using methods recently developed for finite-length optimal digital filters.[12,13] In the results presented here the spacing of data points is 0.15 V. The filter is symmetric of length 29 (i.e., the filter is specified by its 29 nonzero coefficients) and is characterized by exactly linear phase with zero delay. Its frequency response is within 2.85×10^{-3} of 0 below 1 cycle/4.8 V, within 2.85×10^{-4} of 1 above 1 cycle/0.96 V and goes smoothly from 0 to 1 at intermediate frequencies.

The measurement of the dispersion of electronic surface resonances is illustrated in Figs. 1 to 3. The results are for a Ni(001)$c(2\times2)$O surface prepared by exposing initially clean Ni(001) to oxygen as described previously.[7]

Figure 1 shows the raw data. Resonance structure is discernible in Fig. 1 but is brought out much more clearly in the corresponding filtered data shown in Fig. 2. Use of different filters with characteristics close to those described above changes the relative clarity of the resonance signal against the residual background, but basic features of Fig. 2 are not altered.

All of the features in Fig. 2 that appear at accelerating potentials greater than 10 V and that show a systematic dependence on incidence angle are identified as resonances. The resonance line shapes depend on both the energy and direction of incident electrons, but in every case a minimum of reflection coefficient is a prominent and well-defined feature. For the purpose of plotting the dispersion, the resonance center is provisionally taken to be the minimum.

The surface-resonance band structure derived from Fig. 2 is shown by open circles in Fig. 3.

To interpret the results we use a perturbation scheme in which the zeroth-order resonance wave functions represent free-electron motion in directions parallel to the surface. They are products such as

$$\psi(z)\exp[\,i(\vec{k}_{\parallel}+2\pi\vec{g})\cdot\vec{r}\,]. \qquad (1)$$

Here z is the surface-normal coordinate, $\vec{r}$ is a

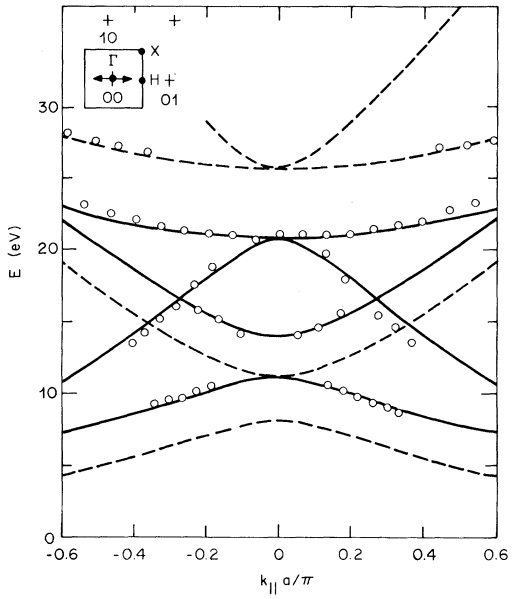

FIG. 3. The surface-resonance band structure of Ni(001)$c(2\times2)$O (electron energy E vs reduced parallel momentum $\vec{k}_{\|}$, open circles) together with the perturbed free-electron surface band structure calculated as described in the text. Full and broken lines correspond to allowed and forbidden resonances, respectively. The inset at top left show the central surface Brillouin zone for Ni(001) (square) with reciprocal-net points (crosses) symmetry points (dots), and an indication of the range of $\vec{k}_{\|}$ spanned by the main figure (arrows). a denotes the Ni(001) unit mesh side (a=2.505 Å).

position vector parallel to the surface, and $\vec{g}$ is a vector of the surface reciprocal net. $\psi(z)$ denotes the lowest-energy bound-state solution of the Schrödinger equation for the crystal potential averaged with respect to $\vec{r}$.[14] The perturbed resonance energies and wave functions are obtained from solutions of the eigenvalue problem for the energy matrix

$$H_{g'-g} = \langle U_{g'-g} \rangle \equiv \int_{-\infty}^{\infty} \psi^* U_{g'-g} \psi \, dz \quad (\vec{g}' \neq \vec{g}) \tag{2a}$$

$$= E + \tfrac{1}{2}|\vec{k}_{\|} + 2\pi\vec{g}|^2 \quad (\vec{g}' = \vec{g}) \tag{2b}$$

where $U_g(z)$ is the two-dimensional Fourier transform of the crystal potential corresponding to reciprocal-net vector $\vec{g}$ and E is the energy eigenvalue corresponding to ψ. Energies are expressed in Hartree atomic units ($\hbar = m = e = 1$) and are referred to the vacuum level as origin.

The surface-resonance band structure calculated using parameter values chosen to fit the data (Table I) are shown as lines in Fig. 3. The full and broken lines refer to resonance states that are, respectively, symmetric and antisymmetric

TABLE I. Surface-resonance band structure parameters (eV). The estimated error in determination of all entries is ±0.2 eV. Subscripts denote components of a reciprocal-net vector referred to the basic vectors of the reciprocal net for Ni(001).

E	$\langle U_{10} \rangle$	$\langle U_{11} \rangle$	$\langle U_{3/2\ 1/2} \rangle$	$\langle U_{20} \rangle$
−1.0	1.5	0.0	0.0	−2.5

with respect to reflection in the plane containing $\vec{k}_{\|}$ and the surface normal. Excitation of the antisymmetric resonances is formally forbidden but is apparently responsible for the weak structure present near 30 V in Fig. 2 (27 eV in Fig. 3).

The agreement between the observed and calculated surface-resonance band structure (Fig. 3) is good.[15] The fit exhibited in Fig. 3 amounts to an empirical determination of the off-diagonal elements of the energy matrix, Eq. (2a) and Table I. The off-diagonal elements are surface-weighted two-dimensional Fourier components of the crystal potential. Synthesis of them yields the surface-weighted potential shown in Fig. 4. The weighting distribution here is the charge density $|\psi(z)|^2$ of the resonance. Because of the limited angular range of the experiment, we have not as yet determined low-index fractional-order Fourier coefficients such as $\langle U_{1/2\,1/2} \rangle$; therefore the potential shown in Fig. 4 is an average over

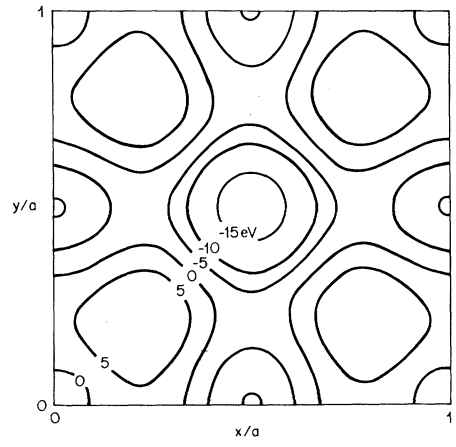

FIG. 4. Surface-weighted effective potential for Ni(001)$c(2\times2)$O. The potential is presented as a contour plot extending over one Ni(001) unit mesh (side a) of the function

$$\sum_{k=-2}^{2} \sum_{l=-2}^{2} \langle U_{kl} \rangle \cos[2\pi(kx + ly)/a],$$

where the coefficient values are taken from Table I.

different Ni(001) unit meshes of the Ni(001)$c(2\times2)$O surface.

The main features of the potential plot in Fig. 4 are a central region of negative potential and regions of positive potential on the unit-mesh diagonals. These features are consonant with what is known about the structure of Ni(001)$c(2\times2)$O surface from LEED intensity analysis.[3] We attribute them to an adsorbed O atom located above the center of the square formed by four adjacent Ni atoms, and to diagonally directed Ni-O bonds, respectively.

Basically the reason that the lateral structure can be extracted directly from experiment is that our procedure in effect selects for observation a region where the potential is weak. In this region the lateral variations of potential cause interactions between two-dimensional free-electron states that are strong enough to measure by the improved technique described in this Letter, but at the same time weak enough to be treated theoretically as a small perturbation.

Some advantages of a method of surface-structure determination based on resonance dispersion measurements are apparent from the example described. The experiment itself is as simple as LEED and much simpler than angle-resolved UPS. With regard to interpretation, no large-scale computations are necessary as is the case for LEED intensity analysis; the lateral structure of the potential is obtained directly from experiment and does not involve computations for trial structures. The interpretation involves the dispersion of only one state and so is inherently simpler than in UPS where the dispersion of both an initial and a final state must be considered.

Helpful discussions with colleagues J. E. Rowe and M. A. Schluter are gratefully acknowledged.

[1]J. B. Pendry, *Low Energy Electron Diffraction* (Academic, New York, 1974).

[2]M. M. Traum, J. E. Rowe, and N. V. Smith, J. Vac. Sci. Technol. 12, 298 (1975).

[3]J. E. Demuth, D. W. Jepsen, and P. M. Marcus, Phys. Rev. Lett. 31, 540 (1973).

[4]K. Hirabayashi, J. Phys. Soc. Jpn. 25, 856 (1968).

[5]S. Miyake and K. Hayakawa, Acta Crystallogr., Sect. A 26, 601 (1970).

[6]E. G. McRae, Surf. Sci. 25, 491 (1971).

[7]E. G. McRae and C. W. Caldwell, Surf. Sci. 7, 41 (1967).

[8]V. Henrich, Surf. Sci. 49, 675 (1975).

[9]P. E. Best, Phys. Rev. Lett. 34, 674 (1975).

[10]E. G. McRae and C. W. Caldwell, Surf. Sci. 57, 63 (1976).

[11]A Hewlett-Packard 9830 calculator and associated interfacing to the experiment are used.

[12]L. R. Rabiner, J. H. McClellan, and T. W. Parks, Proc. IEEE 63, 595 (1975).

[13]J. H. McClellan, T. W. Parks, and L. R. Rabiner, IEEE Trans. Audio Electroacoust. 21, 506 (1973).

[14]Higher-energy bound states might be present but would not be observed in the present experiment because of its limited energy resolution (0.3 eV). Interactions involving the higher-energy states are probably very weak and are neglected here.

[15]The systematic differences near 15 and 23 eV are an experimental artifact that arises as explained previously (Refs. 4 and 7) from the use of a retarding field.

Spiral-Vortex Expansion Instability in Type-II Superconductors*

John R. Clem

Ames Laboratory–ERDA and Department of Physics, Iowa State University, Ames, Iowa 50011

(Received 28 February 1977)

It is shown that a flux vortex, in the presence of a sufficiently large current density applied parallel to its axis, is unstable against the growth of helical perturbations. This instability, which has an analog in magnetohydrodynamics, may play a critical role in current-carrying type-II superconductors subjected to longitudinal magnetic fields.

The behavior of spiral flux vortices in current-carrying type-II superconducting cylinders subjected to longitudinal magnetic fields is not yet completely understood. Still unresolved is the question of the vortex arrangement above the critical current, where a nonzero time-averaged longitudinal voltage and a longitudinal paramagnetic moment coexist. In this case, straightforward critical-state or force-balance calculations, modified to account for spiral vortices, yield a longitudinal moment but do not correctly predict the value of the critical current at which a voltage appears, nor are they capable of providing a satisfactory picture of a flux-flow state with a